EFFECT OF IODINATION ON NF270 NANOFILTRATION MEMBRANE STRUCTURE AND PERFORMANCE

BY

GABRIELLE A. LEVATO

THESIS

Submitted in partial fulfillment of the requirements
for the degree of Master of Science in Environmental Engineering in Civil Engineering
in the Graduate College of the
University of Illinois at Urbana-Champaign, 2017

Urbana, Illinois

Adviser:

Professor Benito J. Mariñas

ABSTRACT

Previous research on free chlorination and chloramination of nanofiltration (NF) and reverse osmosis (RO) polyamide membranes has conclusively shown that these water disinfectants damage the structural integrity of membranes and adversely affect their performance. Secondary oxidants formed from reactions of chlorine disinfectants with bromide and iodide ions have also been found to transform the active layers and affect the performance of fully aromatic polyamide membranes, but the effects on semi-aromatic polyamide membranes are still unreported. This work investigates how exposure to a secondary oxidant, hypoiodous acid (HOI), changes the active layer and rejection performance of the semi-aromatic polyamide membrane NF270. Small coupons of membrane were contacted with HOI solutions at various exposure levels. Exposed coupons were analyzed by X-ray photoelectron spectroscopy, Rutherford backscattering spectrometry, and attenuated total reflectance - Fourier transform infrared spectroscopy to monitor the chemical structure of the membrane active layer. Changes in membrane performance were assessed by performing permeation experiments with Rhodamine-WT (R-WT) and sodium chloride (NaCl) solutions. Structural analysis revealed iodination of the active layer, but at levels that did not result in changes in water permeability or the rejection of R-WT and NaCl.

ACKNOWLEDGMENTS

I would like to express my gratitude to my advisor Professor Benito J. Mariñas for his guidance and support during this project.

Thank you to Lauren Valentino for mentoring me in the field of pressure-driven membrane research and sharing her knowledge and advice throughout my Master's degree. I am also thankful to Seungyun (Aaron) Park for his help running permeation experiments. Additionally, I would like to extend my appreciation to everyone in Mariñas research group who have provided feedback and help along the way.

Thank you to Rick Haasch and Tim Spila at the Frederick Seitz Materials Research Laboratory for the training on materials characterization instruments and help in the analysis of samples.

Most of all, I would like to thank my friends and family for their endless support and love throughout this process.

TABLE OF CONTENTS

CHAPTER 1

INTRODUCTION

Pressure Driven Membranes Systems

Pressure driven membrane processes are promising technologies that can remove components present in freshwater and seawater as small as monovalent ions through physicochemical separation [1]. As Figure 1.1 shows, different classes of pressure driven membranes are capable of varying degrees of contaminant removal. Membranes classified as microfiltration (MF) and ultrafiltration (UF) require less energy for operation and target relatively large contaminants,whereas membranes classified as nanofiltration (NF) and reverse osmosis (RO) require more energy for operation but they are capable of removing small molecules and ions [1]. NF membranes are unique in that they can be manufactured for contaminant removal across a large spectrum. NF membranes can perform similar to UF membranes or RO membranes depending on how they are manufactured; the difference in selectivity comes from the composition and structure of the membrane active layer. NF membranes commonly have a thin-film composites, structure with three distinct layers: a thick polyester backing layer, a thinner polysulfone UF support membrane, and an ultrathin polyamide active layer (Figure 1.2).

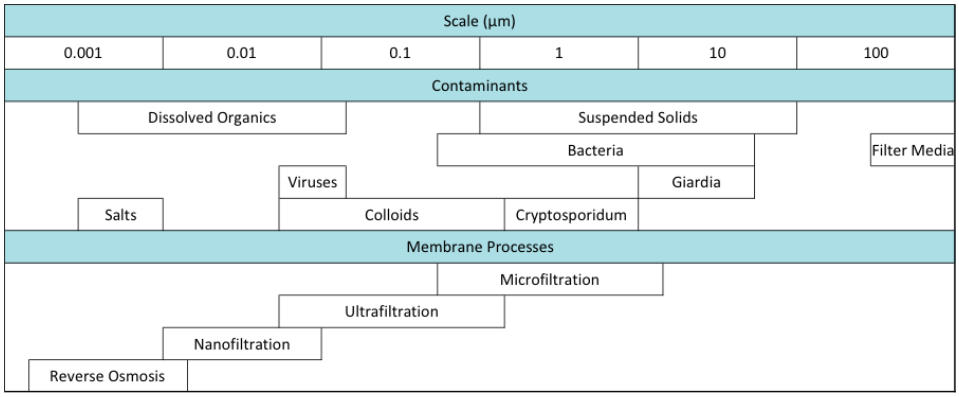

Figure 1.1: Size ranges of pressure driven membrane processes and contaminants [1]

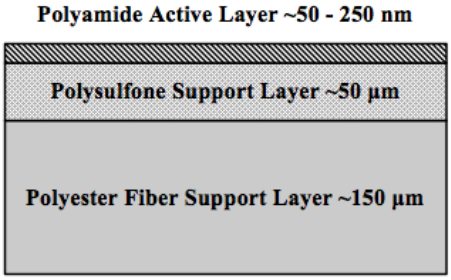

Figure 1.2: Schematic of a membrane cross-section [2, 3, 4]

The active layer is formed by an interfacial polymerization (IP) reaction resulting in either a fully or semi-aromatic polyamide layer. Fully aromatic polyamide membranes are created through the IP reaction of trimesoyl chloride (TMC) and m-phenylene diamine (MPD) with the resulting polymer having a cross-linked structure with the repeating unit shown in Figure 1.3 [5]. Semi-aromatic polyamide membranes are created through an IP reaction of TMC and an aliphatic amine, such as piperazine (PIP) for the membrane used in this study, to form a different cross-linked structure seen in Figure 1.4. Incomplete cross-linking would result in the occurrence of carboxylic and amine groups capable of becoming charged as a function of pH.

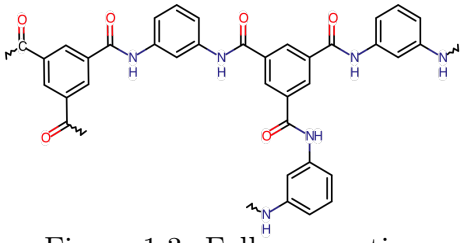

Figure 1.3: Fully aromatic polyamide active layer repeating unit chemical structure,$C_{36}H_{24}N_6O_6$ [5]

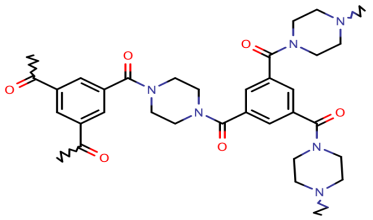

Figure 1.4: Semi-aromatic poly(piperazinamide) active layer repeating unit chemical structure,$C_{30}H_{30}N_6O_6$ [5]

Several properties of the membrane active layer affect membrane performance. Surface roughness, hydrophilic/hydrophobic tendencies and surface charge of the active layer [5, 6] affect the membrane's permeability and selectivity as well as the membrane's susceptibility to fouling [5, 7]. Fouling occurs when unwanted material accumulates on the membrane surface, decreasing the flux through the membrane [6]. Polyamide NF membranes suffer from organic, inorganic and biological fouling issues [6, 8]. Natural organic matter, iron or aluminum and bacteria in water can form organic, inorganic, or biofouling layers, respectively, on the membrane surface. Surface fouling occurs when the negative surface charge associated with incomplete cross-linking is limited, the membrane is hydrophobic or the surface is rough [7]. Fouling results in decreases of both water flux and solute rejection by the membrane, requiring higher maintenance and resulting in higher operational costs for the system to run efficiently [8].

Fully aromatic and semi-aromatic polyamide membranes undergo different reactions with foulants. The semi-aromatic poly(piperazinamide) membrane, NF270 [9] used in this study, has more hydrophilic tendencies and less surface roughness than fully aromatic polyamide counterparts [10], making the semi-aromatic membrane less susceptible to fouling than the fully aromatic membranes. Additionally, differences in active layer chemistry of fully aro-

matic and semi-aromatic polyamide membranes results in different reactivity with chemicals used in membrane system operation. To clean or eliminate fouling layers accumulating on membrane surfaces, it is common to expose the membrane to disinfecting agents [11, 12]. Free chlorine and chloramines and secondary oxidants formed from their reactions with bromide and iodide ions have been shown to react with polyamide active layers. As a result, membrane performance can deteriorate after contact with chlorine disinfectants [4, 11, 13, 14, 15, 16].

The impact of chlorination and chloramination on fully aromatic polyamide membranes is well documented. Previous work has found that both free chlorine and chloramines degrade membrane performance through at least two agreed upon mechanisms: (1) reversible N-chlorination and (2) irreversible ring chlorination [4, 13, 17]. In N-chlorination, the amidic nitrogen takes in chlorine creating N-chloro products that are prone to dechlorination in the absence of the disinfectant. Ring chlorination occurs through either direct aromatic substitution or the Orton rearrangement. In the Orton rearrangement, after the amide nitrogen is chlorinated, there is a rapid intermolecular rearrangement resulting in irreversible chlorination of the amide ring (Figure B.1 in Appendix B) [4, 14, 16].

With semi-aromatic polyamide membranes, different mechanisms of chlorination occur due to the absence of the aromatic ring in the PIP structure. Unlike the fully aromatic polyamide membranes, when exposed to chlorine, the poly(piperazinamide) semi-aromatic membrane incorporates a lower concentration of the halogen signifying that the tertiary nitrogen is less prone to chlorination [11]. In the absence of the amide ring, the chlorine attaches by two mechanisms: (1) reversible N-chlorination of amine nitrogen resulting from incomplete cross-linking (Figure B.2 in Appendix B) and (2) irreversible chlorine

attachment to amide nitrogen resulting in hydrolysis of the C-N bond (Figure B.3 in Appendix B) [11]. The hydrolysis degrades the membrane performance to a smaller extent than ring chlorination, but with quantifiable impact [11].

In addition to directly impacting the performance of polyamide membranes, chlorination also indirectly affects membrane performance via interactions with naturally occurring compounds found in water. Both freshwater and seawater contain natural components that can also react with chlorine disinfectant. For example, iodide (I^-) and bromide (B^-) can both be oxidized by free chlorine or chloramines to become hypoiodous acid (HOI) and hypobromous acid (HOBr) or bromochloramine (NHBrCl) by the reactions summarized in Table 1.1. The impact of oxidized iodide and bromide species on fully aromatic polyamide membranes has been assessed. Both halogens attack the fully aromatic structure, through N-halogenation or ring halogenation, resulting in membrane degradation [4, 18]. Interestingly, bromide species appear to react at a similar magnitude as chlorine compounds [4, 15, 18], whereas HOI showed less influence on membrane performance [4, 18]. Limited investigation has been conducted on reactions of semi-aromatic polyamide membranes to secondary oxidants like HOBr and HOI.

Table 1.1: Possible reactions between free chlorine, monochloramine, bromide, and iodide compounds in water

Reaction	**Rate Constant**	**Source**
$HOCl + Br^- \longrightarrow HOBr + Cl^-$	$5.1 * 10^5$ $M^{-1}H^{-1}$	[19]
$HOBr + NH_2Cl \longrightarrow NHBrCl + H2O$	'fast'	[19]
$HOCl + I^- \longrightarrow HOI + Cl-$	$4.3 * 10^8$ $M^{-1}s^{-1}$	[20]
$NH_2Cl + I- \longrightarrow HOI + Cl^- + NH_3$	$2.4 * 10^{10} * [H^+]$ $M^{-2}s^{-1}$	[20]

Chlorine Oxidation of Iodide

Iodide (I^-) can be oxidized by either free chlorine or monochloramine during water treatment. Free chlorine is a strong oxidant and common disinfectant that is prone to combine with natural organic matter in water to form disinfection by-products (DBPs) [21]. Due to the high occurrence of regulated brominated and chlorinated DBPs, many water treatment facilities have started to use monochloramine, a weaker disinfectant [21]. Whereas free chlorine will oxidize I^- to iodate (IO_3^-), monochloramine will oxidize (I^-) to HOI [20]. The formed HOI reacts with natural organic matter to form iodinated DBPs, which are not yet regulated, as well as with the polyamide membranes. Figure 1.5 below shows the fate of iodine after monochloramine exposure.

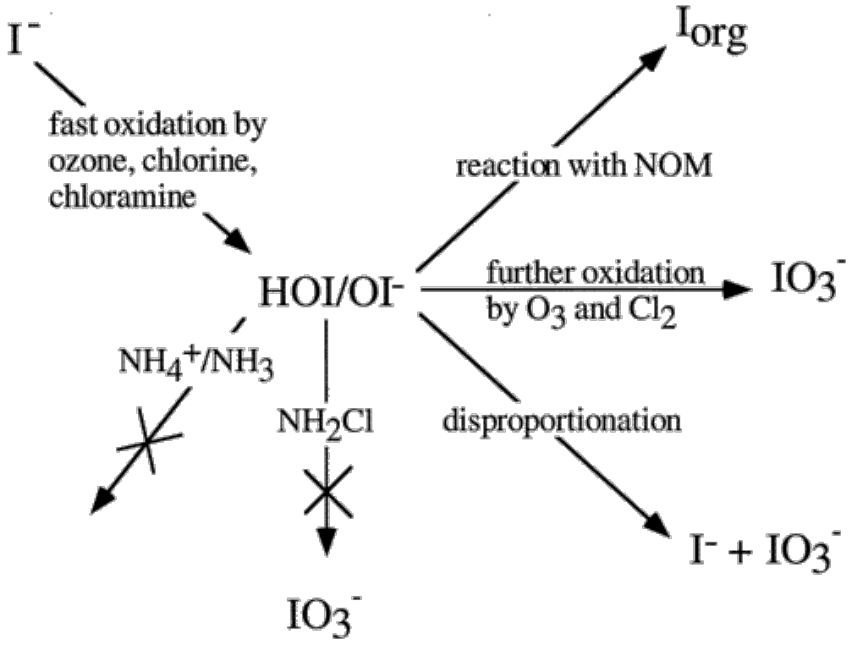

Figure 1.5: Fate of iodine during oxidative water treatment [20]

XPS and RBS

X-ray photoelectron spectroscopy (XPS) and Rutherford backscattering spectrometry (RBS) are both analytical instruments used to obtain elemental information about material composition. XPS analysis uses an X-ray beam to excite electrons in the sample up to six nanometers in depth [3]. The binding energy (BE) of elements in the sample are calculated from the photon energy of the X-ray source ($h\nu$), the measured specific kinetic energy of the excited electrons (KE), and the instrument's calibration (ϕ_{spec}) via Eq.1.1:

$$BE = h\nu(known) - KE(measured) - \phi_{\text{spec}}(calibrated) \tag{1.1}$$

Figure 1.6 shows a survey scan of all elements, except hydrogen, in a pristine (not exposed to any solution) NF270 membrane. The raw data can be interpreted using CasaXPS software to obtain information in terms of counts per second (CPS) as a function of binding energy. High resolution scans can be obtained for elements of interest, which allow the user to determine the area of each element peak. With this information, relative atomic concentration percent of each element can be used to determine the composition of the sample. Although XPS is capable of providing surface level compositional data, it cannot provide the depth-average composition of the membrane.

Alternatively, RBS analysis is capable of layered compositional data acquisition to a depth of about 2 μm into the sample [3]. This instrument can measure the average atomic composition as a function of the depth of the sample. The RBS uses an ion scattering technique that results from elastic collisions between the ion beam, helium in this study, and sample nuclei. When the beam hits the sample, the helium ions are scattered with specific energies that correspond to individual atoms. Based on the mass and depth of the atom, the

peaks and plateaus shown in Figure 1.7 are obtained. RBS spectra are analyzed with the SIMNRA software to obtain elemental composition from the height of peaks and plateaus. The RBS' ability to relay depth information is demonstrated in Figure 1.7 with a sulfur plateau, representing the polysulfone support layer ($C_{27}H_{26}O_6S$), while the XPS scan shows no sulfur peak (~200 - 250 eV range).

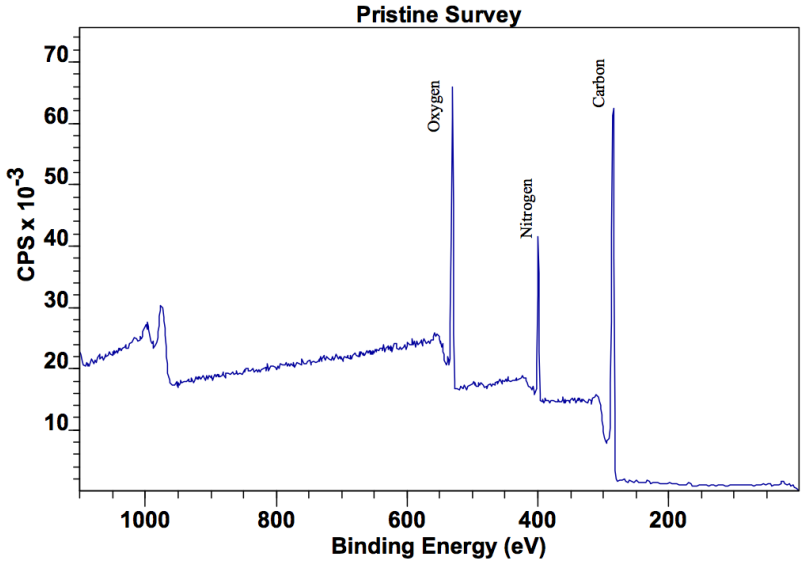

Figure 1.6: Pristine NF270 XPS characterization. Elements are labeled as they appear in the spectra

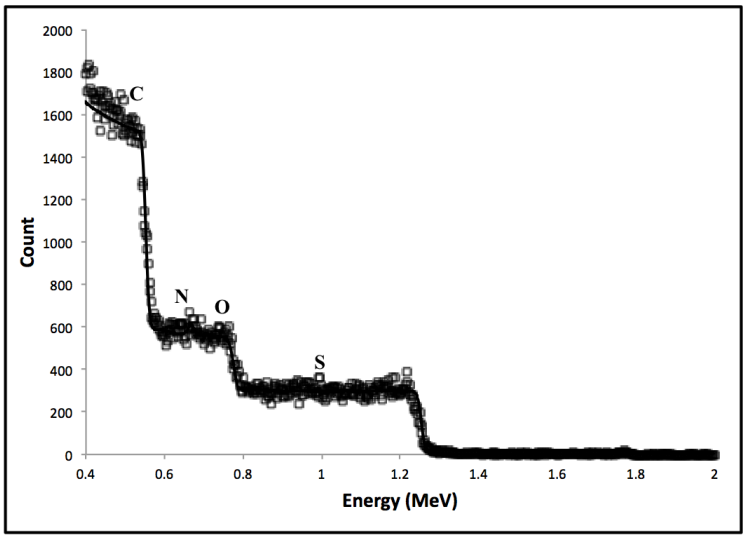

Figure 1.7: Pristine NF270 RBS characterization. Elements are labeled as they appear in the spectra. Raw data points obtained during RBS analyses are denoted using symbols, and simulated data curves obtained using SIMNRA are illustrated with solid lines

Objectives

The primary objective of this study is to understand the physical or structural changes occurring in the membrane active layer resulting from the exposure to varying concentrations of HOI. Structural changes are assessed through XPS and RBS analyses for elemental compositional data of membranes, which provides insight into the location of the iodine within the semi-aromatic polyamide structure. These techniques are paired with ATR-FTIR, which assesses changes in functional groups of the polymeric membrane.

An additional objective is to assess the membrane performance before and after exposure to HOI. Membrane permeation experiments using aqueous solutions of water, Rhodamine-WT (R-WT) and sodium chloride (NaCl) as feed solutions are conducted to understand how membrane rejection capability changes with increasing exposure to HOI.

CHAPTER 2

MATERIALS AND METHODS

Membranes Permeation Experiments

Permeation experiments were performed with coupons (44.5 mm diameter; 13.4 cm^2 effective area) cut from the thin-film composite membrane NF270 [9]. Membrane coupons were installed in 50-mL amicon stirred cells [22] and tested with aqueous feed solution of Rhodamine-WT (R-WT) solution or sodium chloride (NaCl).

Membrane Characterization

Membrane coupons (5 mm x 5 mm for XPS and 25 mm x 25 mm for RBS) were exposed to target concentration (see next section) of secondary oxidizing agent HOI or blank solution, rinsed in a 10^{-6} dilution of sodium iodide (NaI) and dried for at least 24 hours prior to instrument analysis. All membranes were rinsed in 18 MΩ-cm Milli-Q water for at least 24 hours prior to use.

Chemicals

Hypoiodous Acid (HOI)

HOI solutions were prepared by reacting NaI with monochloramine (NH_2Cl). Concentrations used can be found in Table A.3. NaI solutions were prepared

by dissolving sodium iodide in phosphate buffer solution. NH_2Cl solutions were prepared as stated below.

Monochloramine (NH_2Cl)

A monochloramine stock solution of 1000 mg/L as Cl_2 was prepared daily by mixing equal volumes of 0.75 M ammonium chloride (NH_4Cl) and 0.706 M hypochlorous acid (HOCl) solutions in 18 MΩ-cm Milli-Q water. The HOCl solution was slowly pipetted into the NH_4Cl solution under continuous mi-ing by magnetic stirring. Resulting NH_2Cl solutions had a target N:Cl ratio of 1.1:1. The actual final concentration of NH_2Cl was determined by mea-suring the UV absorbance at 243 nm in a ultra-violet visible light (UV-Vis) spectrophotometer (Shimadzu UV-2550). Absorbance values were converted to concentrations with the Beer-Lambert law equation using a NH_2Cl molar absorptivity of 433 cm^{-1}. Table A.1, Table A.2 and Tables A.4 - A.7 display sample calculations and raw data in NH_2Cl preparation.

Phosphate Buffer

Phosphate buffer solutions were prepared by dissolving disodium phosphate salt in 18 MΩ-cm Milli-Q water. The target buffer concentration was 15 mM and the pH was adjusted to 8.3 using HCl or NaOH as needed.

Analytical Techniques

Ion Chromatography

A Thermo Scientific Dionex ICS-2100 Ion Chromatography (IC) was used to analyze permeation samples from NaCl experiments. Duplicate samples were

filtered through 0.45 μm filters [23] and placed into 1.5 mL autosampler vials [24].

Spectrofluorometry

A Shimadzu RF-5301PC Spectrofluorophotometer was used to analyze permeation samples from R-WT experiments. R-WT samples underwent a 1:10 dilution for permeate samples and 1:1000 dilution for feed samples in order to obtain readings in the RF-5301PC. The excitation wavelength was set to 550 nm and the emission wavelength was set to 580 nm for proper analysis of R-WT fluorescence. Triplicates of each sample were taken with the RF-5301PC.

X-ray Photoelectron Spectroscopy (XPS)

XPS analyses were performed with a Kratos Axis ULTRA spectrometer equipped with a MgKα X-ray source (hν = 1253.6 eV). Membrane samples were cut into 5 mm x 5 mm squares and mounted on double sided copper tape [25]. Survey scans and high resolution scans for oxygen, nitrogen, carbon and iodine were obtained for all XPS samples.

Rutherford Backscattering Spectrometry (RBS)

RBS analyses were performed with a 3SDH NEC Pelletron. A stable, 2.0 MeV helium (He+) beam with a 3 mm diameter and 50 nA current were used to analyze all samples. Membrane samples were cut into 25 mm x 25 mm squares and mounted on double sided aluminum tape [26]. At least 1000 counts of carbon were collected for each sample. The system was set up with incident, exit, and scattering angles of 22.50°, 52.50°, and 150.0°, respectively. Using SIMNRA software, raw data was fit with a simulated line that was normalized

to the sulfur plateau as previous studies have shown [3, 4]

Attenuated Total Reflection-Fourier Transform Infrared Spectroscopy (ATR-FTIR)

ATR-FTIR analyses were performed with a Nexus 670 FTIR spectrometer (Thermo Nicolet Corporation) equipped with a smart golden gate single-reflection diamond ATR accessory, DTGS-KBR detector, KBr beam-splitter and an IR source of 45°. Spectrum software was programmed to take 50 scans in 0.1 increments over a 400 - 4000 nm wavelength range at a resolution of 2 cm^{-1}. Data was normalized to a peak at 1488 cm^{-1} that corresponds to the polysulfone support layer that is known to remain unchanged from chlorine exposure [12].

CHAPTER 3

RESULTS AND DISCUSSION

Structural Changes

XPS

Pristine and iodinated membrane coupons were first analyzed by XPS to determine the atomic concentration of pristine and iodinated membranes near the exposed surface of the membrane active layer. Two iodine peaks were visible in the 616-620 eV range and the 628-632 eV range as seen in the high resolution scans in Figures 3.1a and 3.1b. These scans show that the CPS values increased with increasing exposure to HOI in the range of 0 - 300 mM·h investigated. The presence of iodine peaks indicates halogenation of the polyamide active layer. Absence of the iodine peaks in both the pristine membranes and control membrane experiments, membranes only exposed to NaI solution, supports the conclusion that halogenation of the membranes is a result of the interaction with HOI produced from oxidation of iodide by monochloramine.

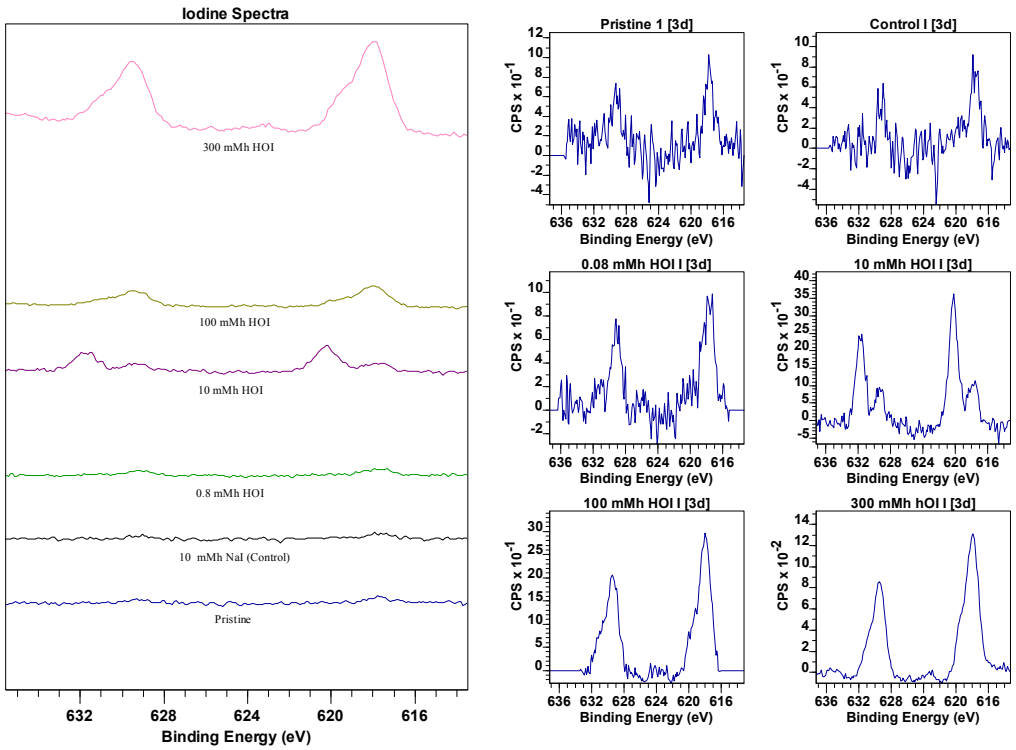

(a) (b)

Figure 3.1: (a) All high resolution XPS scans of the iodine spectra (b) Individual high resolution XPS scans of iodine spectra

Using CasaXPS, concentrations of iodine within the membrane could be assessed. Figure 3.2 displays the relationship between HOI exposure and iodine incorporation. There is a rapid growth in iodine uptake as HOI exposure increases, but the relative percent of iodine within the membrane structure remains relatively low; exposure to 300 mM·h HOI results in only 0.40% iodine. Taking the known percentages of iodine in the membrane, summarized in Table 3.1, and knowing the structure of the semi-aromatic poly(piperazinamide) membrane (Figure 1.4), approximately 1.4-28.0 percent of the polyamide repeating unit has one iodine attached or $C_{30}H_{29}N_6O_6I$, while the rest remains in the original form $C_{30}H_{30}N_6O_6$. This suggests that most repeating units of the semi-aromatic polyamide do not have any halogens attached and at most, have one iodine after an exposure to HOI of 300 mM·h.

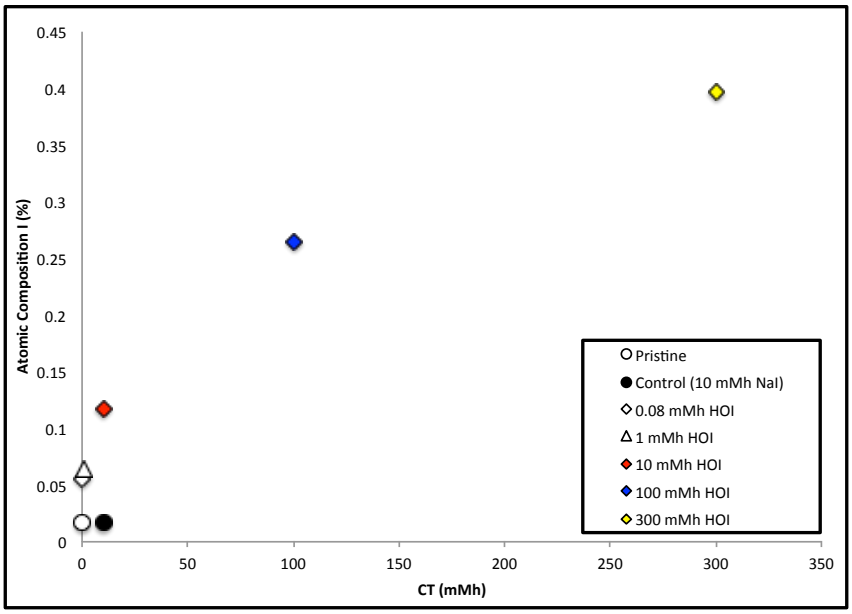

Figure 3.2: XPS results of atomic percent of iodine incorporated into NF270 structure

Table 3.1: Atomic percent of oxygen, nitrogen, and iodine found in pristine and exposed membrane samples for both XPS and RBS

	XPS	RBS	XPS	RBS	XPS	RBS	XPS	RBS
CT (mM·h HOI)	%O		%N		O/N Ratio*		%I	
0	14.95	5.00	12.07	3.00	1.24	1.67	0.02	0.00
10	15.82	5.00	11.55	3.00	1.37	1.67	0.12	0.05
100	15.86	5.00	12.16	3.00	1.30	1.67	0.27	—
300	15.42	5.00	11.99	3.00	1.29	1.67	0.40	0.32

*O/N ratio describes the degree of crosslinking in membrane; Values close to 1 are completely crosslinked and values close to 2 are completely linear

RBS

Following the XPS analysis, RBS was utilized to gain more information about iodine incorporation into the polysulfone support layer.

The first set of RBS analyses were conducted on membranes exposed to 0 (pristine), 10 and 300 mM·h HOI. These membranes were prepared in the same manner as those analyzed with XPS, through exposure to the HOI solution followed by a sodium iodide rinse. An iodine peak is very visibly seen at 1.8 MeV in the survey scan, Figure 3.3a. Zooming into that region in Figure 3.3b, the RBS data supports that exposure to higher concentrations of HOI result in higher iodine incorporation into the membrane (Table 3.1). The lower atomic concentration obtained by RBS (0.05% and 0.32%) compared to those observed with XPS samples (0.12% and 0.40%) reveals a lack of homogeneity in the iodine profile with the concentration near the active layer surface obtained by XPS being higher than the average in the entire active layer obtained by RBS. The greater depth characterization by RBS also allows for small amounts of iodine incorporated into the polysulfone support to be seen. The increase in the plateau leading into the iodine peak, seen clearly in Figure 3.3b, represents the iodine attached to the polysulfone support. The percentages of iodine present in the support layers as a function of HOI exposure are summarized in Table 3.2.

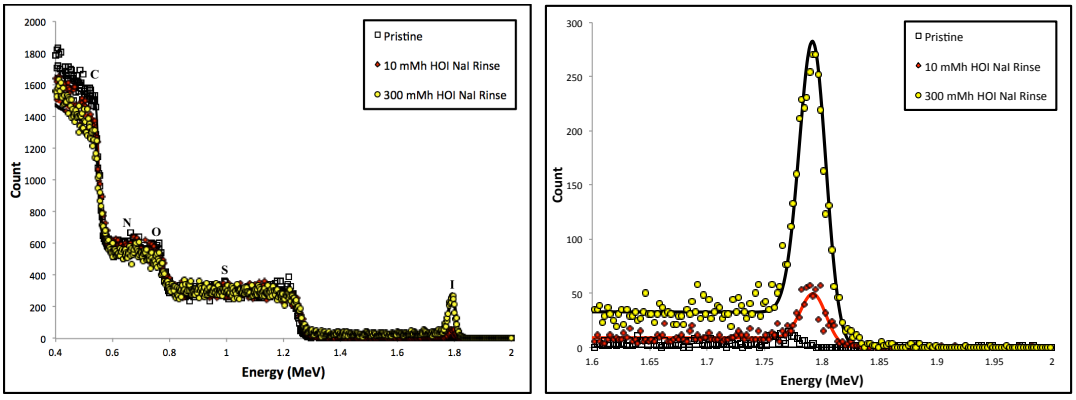

(a) (b)

Figure 3.3: RBS analysis of pristine, 10 mM·h HOI and 300 mM·h HOI exposed membranes with NaI rinse. (a) Full spectra (b) iodine spectra

Table 3.2: Iodine concentrations in active and support layers from RBS analysis for permeation and non permeation experiments

	No Permeation		**Permeation**	
	NaI rinse	**NaCl rinse**	**R-WT perm**	**NaCl perm**
10				
Active Layer	0.053%	0.045%	0.02%	0.03%
Support Layer	0.0043%	0.004%	0.003%	0.003%
100				
Active Layer	—	0.11%	0.07%	0.055%
Support Layer	—	0.005%	0.006%	0.005%
300				
Active Layer	0.32%	0.225%	0.11%	0.06%
Support Layer	0.018%	0.01%	0.01%	0.007%

The stability of the iodine in the membranes was then assessed. Exposed membranes underwent permeation experiments to understand the effect of iodination on organic and salt rejection. As shown in Figures 3.4a and 3.4b and Figures B.5 and B.6 in the appendix, RBS analysis of exposed membranes after roughly 50 hours of permeation, showed lower iodine concentrations compared with those observed for the membranes before permeation experiments Figures 3.3a and 3.3b.

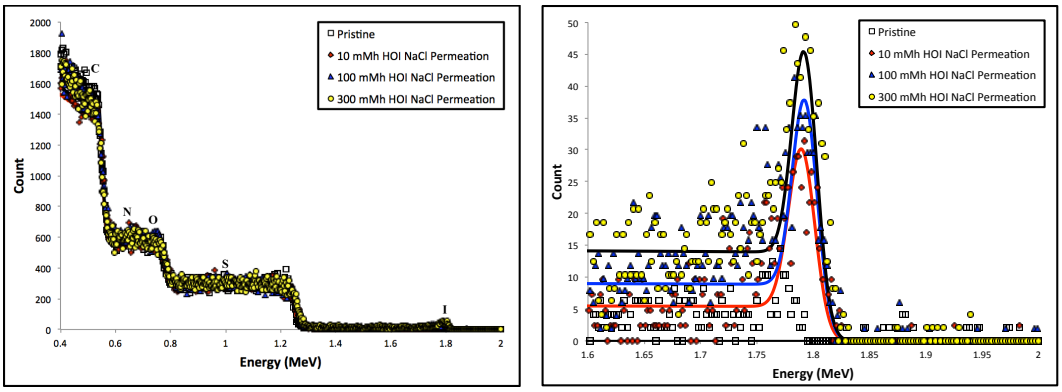

(a) (b)

Figure 3.4: RBS analysis of pristine, 10, 100, and 300 mM·h HOI exposed membranes followed by NaCl permeation. (a) Full spectra (b) iodine spectra

Over the course of the permeation experiment, the iodine is removed from the membrane. A control test was performed to understand whether the iodine was being removed simply due to the amount of time feed solution passed through the membrane or if the feed solution, in particular the chloride ion, was responsible. Instead of rinsing the exposed membrane with the NaI solution, the membrane was rinsed in a 400 mg/L NaCl solution (the same concentration used in permeation experiments) for 30 minutes. Figure 3.5 below and Figures B.7 and B.8 in the appendix show the permeation and rinse analysis results for 300,10, and 100 mM·h HOI, respectively. Graphically and from the values found in Table 3.2, there is a decline in iodine uptake after the NaCl rinse. This would indicate that the solution plays a role in the release of iodine from the membrane, and the prolonged exposure in the permeation experiments removes the iodine almost entirely.

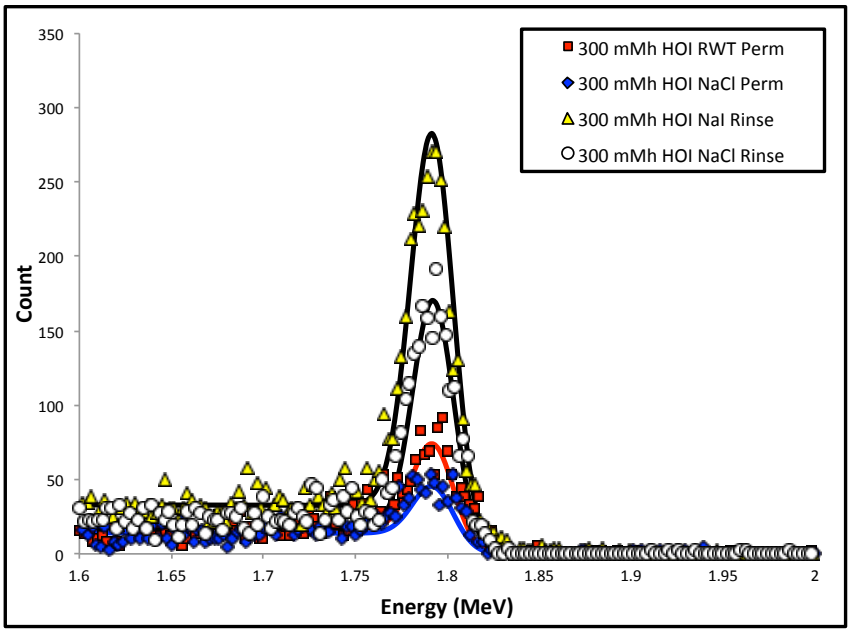

Figure 3.5: RBS analysis of 300 mM·h HOI exposed membranes after NaI rinse, NaCl rinse, R-WT permeation, and NaCl permeation

The instability of iodine attachment to the semi-aromatic polyamide structure indicates that the iodine is attaching in a reversible location, such as the non-crosslinked nitrogen atoms. To verify that no irreversible modifications occurred in the membrane after iodine exposure, ATR-FTIR analyses were conducted. Pristine membranes and membranes exposed to 10, 100, and 300 mM·h HOI showed no changes in any bonds as seen in Figure 3.6.

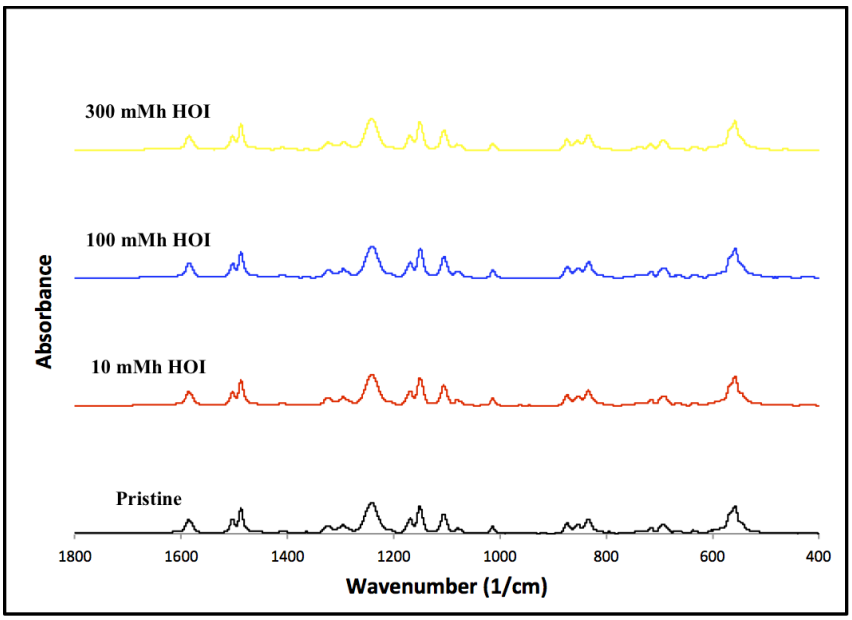

Figure 3.6: FTIR analysis of pristine, 10, 100, and 300 mM·h HOI exposed membranes

In previous studies in which NF270 membrane samples were exposed to the stronger oxidizing agent, free chlorine, the semi-aromatic structure showed a flattening of the amide I band (1630 cm^{-1}) in ATR-FTIR spectra with increased exposure to the halogen [12]. This flattening occurs due to the hydrolysis of the C-N bonds of the piperazine structure. The C-N hydrolysis results in increased oxygen and less cross-linking and ultimately changes the membrane composition and performance. None of these changes occur in membranes exposed to HOI, supporting the conclusion that iodine is not a strong enough oxidant to facilitate the hydrolysis of the C-N bonds and therefore it only attaches to an easily reversible position such as on the non-crosslinked nitrogen.

Membrane Performances

Transport Model

Performance for the NF270 membrane was characterized by inputting raw data found in Appendix C.1 - C.12 into the solution-diffusion model Eq. 3.1 [27]

$$Rejection = 1 - \frac{c_{\mathrm{p}}}{c_{\mathrm{f}}} = \frac{100}{1 + (\frac{B}{1-\alpha} \cdot \frac{1}{J_{\mathrm{v}}} + \frac{\alpha}{1-\alpha}) e^{\frac{J_{\mathrm{v}}}{k}}} \tag{3.1}$$

Where B is the solute transport parameter, α is the total product water flux due to feed solution leakage, J_{v} is the solution flux, and k is the solute mass transfer coefficient. This equation takes into account three distinct mechanisms controlling membrane performance: (1) diffusion through the membrane, (2) advection through the membrane, and (3) concentration polarization in the feed solution laminar film adjacent to the exposed active layer interface [27]. Concentration polarization refers to the buildup of solute within the laminar film next to the membrane surface due to membrane selectivity, which results in higher solute concentration next to the membrane wall compared to that in the bulk feed solution and corresponding lower water flux and lower solute rejection [28].

The values for intrinsic rejection, J_{v} and k are found experimentally. Solute rejection is calculated from permeate and feed concentrations (c_{p} and c_{f}) found for R-WT or NaCl. The water flux is calculated from gravimetric measurements as solution passes through the membrane. The solute mass transfer coefficient for R-WT, $k = 0.9$ m/d, was obtained by fitting permeation data, and $k = 2.6$ m/d was calculated from from the relationship between solute mass transfer coefficients and diffusion coefficients seen in Eq. 3.2 [27].

$$\frac{k_{\text{NaCl}}}{k_{\text{R-WT}}} = \left(\frac{D_{\text{NaCl}}}{D_{\text{R-WT}}}\right)^{\frac{2}{3}} \tag{3.2}$$

The values for α and B must be determined through a Sigmaplot regression using Eq. 3.1.

R-WT Experiments

R-WT was used as a surrogate for organic solutes to assess the membranes rejection capabilities before and after exposure to iodine. Two interesting results are observed from the R-WT performance data. First, the α, B and k parameters determined do not properly represent how these NF270 membranes performed, and second, the iodine exposure resulted in no measureable change in membrane performance.

In Figures 3.7a, 3.8a, and 3.9a, the raw data points (Tables C.1, C.3 and C.5) were run through a Sigmaplot regression to obtain viable values for α and B, with the known value of k for R-WT.

The parameters found for α and B (Table 3.3) using the low flux data do not fit the higher flux points of the experimental data. The front portion of the curve (approximately 0.0 - 0.4 m/d) represents the diffusive aspect of the membrane, whereas, the later portion of the curve represents the advective portion. The decline in the fitting lines shows the role concentration polarization is supposed to have on membrane performance. This fitting shows that concentration polarization is not influencing the advective transport of solute through the membrane in the higher flux points. Since the values of α and B are intrinsic to the membrane, the only variable that can be adjusted to improve the fit is the k value. Since k signifies the solute mass transfer across the membrane and it is clear that the solute transfer changes over the course

of the experiment, the k value would need to be adjusted to account for the change in concentration polarization. Figures 3.7b, 3.8b, and 3.9b, show the new rejection fittings when the Sigmaplot regression was processed again with α and B constrained to determine the correct value for k. All parameter values can be found in Table 3.3.

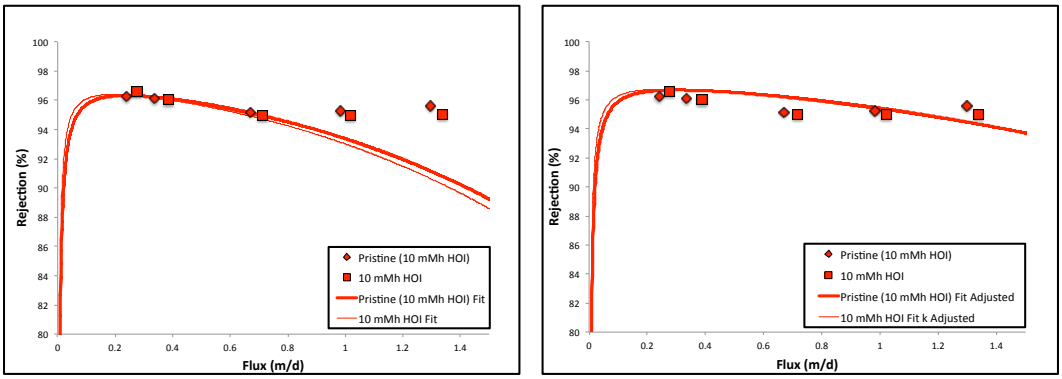

(a) (b)

Figure 3.7: R-WT Rejection: 10 mM·h HOI (a) $k = 0.9$ (b) Adjusted k values

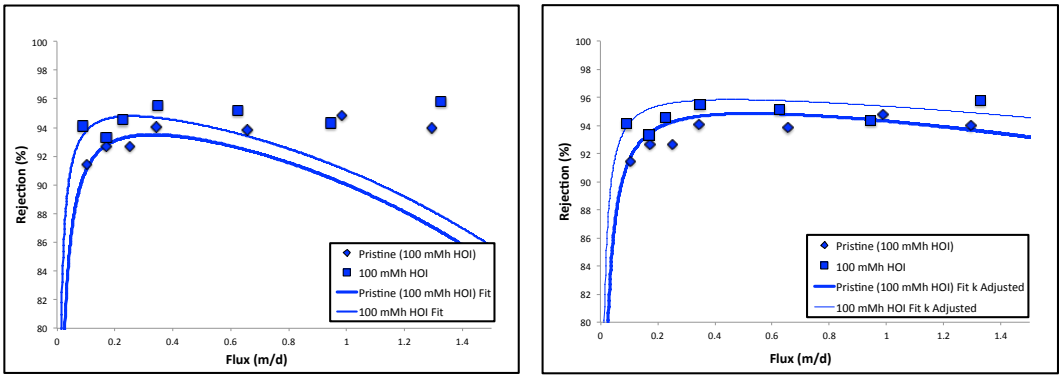

(a) (b)

Figure 3.8: R-WT Rejection: 100 mM·h HOI (a) $k = 0.9$ (b) Adjusted k values

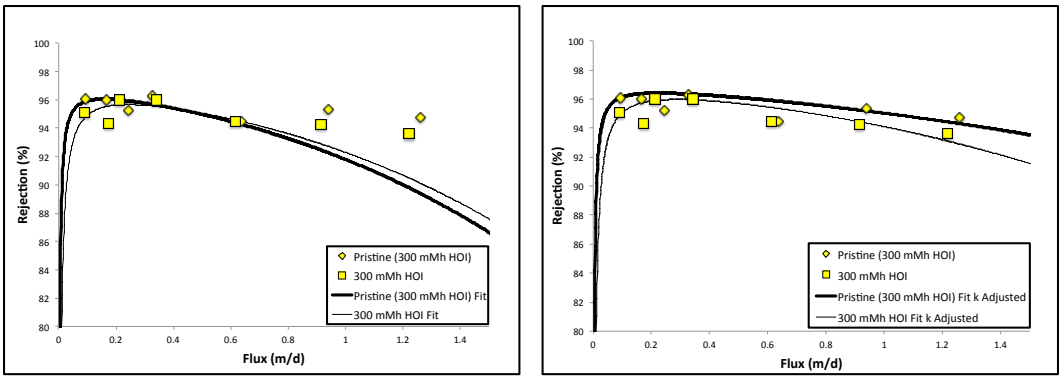

(a) (b)

Figure 3.9: R-WT Rejection: 300 mM·h HOI (a) $k = 0.9$ (b) Adjusted k values

Table 3.3: Membrane water and solute transport parameters for R-WT rejection

	R-WT				
CT(mM·h HOI)	$A(m/(d*MPa))$	$B(m/d)$	α	$k(m/d)$ *	$k(m/d)$ **
0 (Pristine of 10)	3.289	0.001817	0.02107	0.9	1.386
10	3.589	0.001265	0.02293		1.502
0 (Pristine of 100)	3.297	0.005596	0.02983		1.996
100	3.369	0.002945	0.02861		2.485
0 (Pristine of 300)	3.278	0.000925	0.02771		1.736
300	3.240	0.002210	0.02463		1.212

A = water transport parameter

* k value for Figure 3.7a,Figure 3.8a, and Figure 3.9a

** k value for Figure 3.7b, Figure 3.8b, and Figure 3.9b

The water permeability through the membrane is shown in Figure 3.10 and the corresponding water permeation parameters (slopes of the regression lines in Figure 3.10) are summarized in Table 3.4. Similar to the R-WT rejection data, there is no measurable change in the water flow through the membrane.

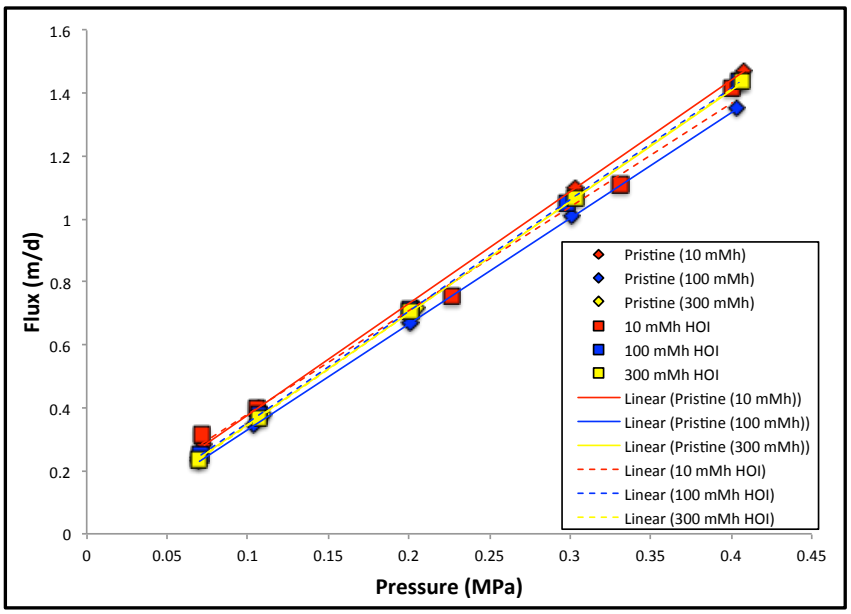

Figure 3.10: R-WT water permeation for pristine and exposed membranes

Table 3.4: R-WT water permeation parameters

	CT (mM·h HOI)	**slope**	**R^2**
R-WT	0 (Pristine of 10)	3.6207	0.99941
	10	3.4632	0.99006
	0 (Pristine of 100)	3.4040	0.99997
	100	3.5390	0.99997
	0 (Pristine of 300)	3.5152	0.99994
	300	3.6469	0.99992

NaCl Experiments

NaCl was used to assess the membranes salt rejection capabilities before and after exposure to iodine. Since the salt molecules are smaller than the R-WT molecules, diffusion is the dominant process controlling salt rejection, as seen by the curves in Figure 3.11. When the raw data points (Tables C.7 - C.12) were processed through the Sigmaplot regression, values for B, the parameter

representing diffusion, were found but values for α could not be determined. Since the α parameter signifies advection, and advection represents the imperfections through the membrane, the average of the advective values found in the R-WT experiments was used as the value of α for the NaCl experiments. Similar to the R-WT experiments, there was no observable change in membrane performance after iodination.

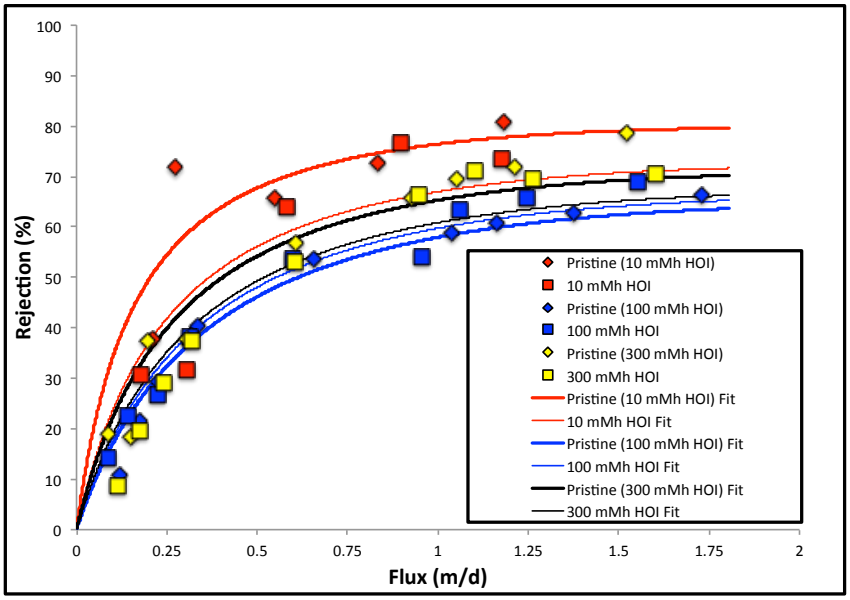

Figure 3.11: NaCl rejection for pristine and exposed membranes

Table 3.5: Membrane water and solute transport parameters for NaCl rejection

	NaCl			
CT(mM·h HOI)	$A(m/(d*MPa))$	$B(m/d)$	α	$k(m/d)$
0 (Pristine of 10)	3.024	0.1787	0.0258	2.6
10	3.072	0.301		
0 (Pristine of 100)	3.391	0.4556		
100	3.228	0.4212		
0 (Pristine of 300)	3.058	0.3264		
300	3.304	0.4008		

A = water transport parameter

The water permeability observed for the NaCl experiments was not affected by HOI exposure as seen in Figure 3.12 and Table 3.6.

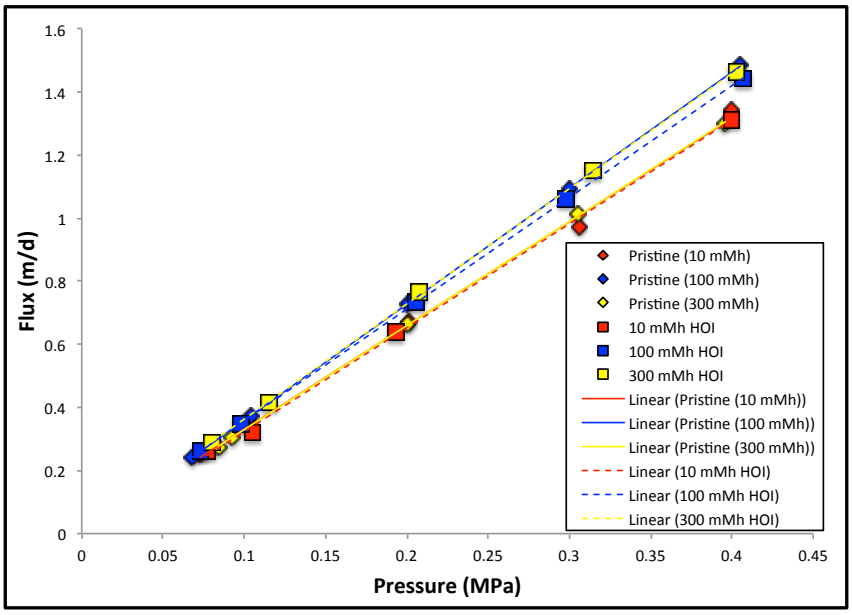

Figure 3.12: NaCl water permeation for pristine and exposed membranes

Table 3.6: NaCl water permeation parameters

	CT (mM·h HOI)	**slope**	**R^2**
NaCl	0 (Pristine of 10)	3.2970	0.99733
	10	3.2726	0.99911
	0 (Pristine of 100)	3.6507	0.9999
	100	3.5550	0.99997
	0 (Pristine of 300)	3.2997	0.99979
	300	3.5199	0.99981

The results of the permeation experiments revealed that HOI exposure up to 300 mM·h had no effect on membrane performance. This observation is consistent with the membrane structure analysis experiments; since no bond breakage within the membrane structure is observed and the iodine is released form the membrane throughout the course of the permeation experiments.

CHAPTER 4

CONCLUSIONS

This research focuses on the effects of HOI exposure on the semi-aromatic poly(piperazinamide) membrane structure and performance. Previous research has been conducted on the influence of chlorination and chloramination of both semi-aromatic and fully aromatic polyamide membranes, as well as limited research on bromination and iodination on fully aromatic membranes. Due to the unique performance change associated with iodination of fully aromatic polyamide membranes, the present study is undertaken to understand whether the semi-aromatic polyamide would behave in the same manner.

Using techniques such as XPS, RBS, and ATR-FTIR to analyze the structural changes iodination had on the semi-aromatic membrane in conjunction with performance permeation experiments to track changes in organic and salt rejection, the effect of iodination is assessed.

The results of the structural analysis determined that increasing exposure to HOI resulted in increased iodine incorporation to both the active and support membrane layers. This iodination was not stable in the membrane structure, and throughout the permeation process, nearly all of the iodine was released from the membrane. This indicates that the iodine attaches in an easily reversible position, such as the non-crosslinked nitrogen atoms.

In the permeation experiments, raw data was fit with the solution-diffusion model to understand the role of diffusion, advection, and concentration polarization in the membrane. Before and after iodination, the membrane parame-

ters and rejection capabilities did not change. This finding is consistent with the structural analysis data.

In conclusion, unlike chlorine, iodine is not a strong enough oxidant to cause any structural or performance changes in the semi-aromatic poly(piperazinamide) NF270 membrane for HOI exposures up to 300 mM·h. Although a small amount of halogenation occurs, the bond location does not inhibit the membrane performance and is easily reversible over a short period of time. It would be beneficial to conduct further research on this topic to understand how higher concentrations of iodine influence the membrane performance and to gain a better understanding about how and why iodine is released from the semi-aromatic membrane.

REFERENCES

[1] J. K. Edzwald, *Water Quality and Treatment A Handbook on Drinking Water*. McGrawHill, 2010.

[2] R. J. Petersen, "Composite reverse osmosis and nanofiltration membranes," *Journal of membrane science*, vol. 83, no. 1, pp. 81–150, 1993.

[3] O. Coronell, B. J. Marinas, and D. G. Cahill, "Depth heterogeneity of fully aromatic polyamide active layers in reverse osmosis and nanofiltration membranes," *Environmental science & technology*, vol. 45, no. 10, pp. 4513–4520, 2011.

[4] L. Valentino, T. Renkens, T. Maugin, J.-P. CroueÌĄ, and B. J. Mariñas, "Changes in physicochemical and transport properties of a reverse osmosis membrane exposed to chloraminated seawater," *Environmental science & technology*, vol. 49, no. 4, pp. 2301–2309, 2015.

[5] C. Y. Tang, Y.-N. Kwon, and J. O. Leckie, "Effect of membrane chemistry and coating layer on physiochemical properties of thin film composite polyamide ro and nf membranes: I. ftir and xps characterization of polyamide and coating layer chemistry," *Desalination*, vol. 242, no. 1-3, pp. 149–167, 2009.

[6] A. Al-Amoudi and R. W. Lovitt, "Fouling strategies and the cleaning system of nf membranes and factors affecting cleaning efficiency," *Journal of Membrane Science*, vol. 303, no. 1, pp. 4–28, 2007.

[7] C. Y. Tang, Y.-N. Kwon, and J. O. Leckie, "Fouling of reverse osmosis and nanofiltration membranes by humic acidâĂŤeffects of solution composition and hydrodynamic conditions," *Journal of Membrane Science*, vol. 290, no. 1, pp. 86–94, 2007.

[8] K. Doederer, M. J. Farré, M. Pidou, H. S. Weinberg, and W. Gernjak, "Rejection of disinfection by-products by ro and nf membranes: influence of solute properties and operational parameters," *Journal of Membrane Science*, vol. 467, pp. 195–205, 2014.

[9] "Dow filmtec nf270-400/34i." [Online]. Available: http://www.dow.com/webapps/include/GetDoc.aspx?filepath=liquidseps/pdfs/noreg/609-50107.pdf

[10] C. Y. Tang, Y.-N. Kwon, and J. O. Leckie, "Effect of membrane chemistry and coating layer on physiochemical properties of thin film composite polyamide ro and nf membranes: Ii. membrane physiochemical properties and their dependence on polyamide and coating layers," *Desalination*, vol. 242, no. 1-3, pp. 168–182, 2009.

[11] V. T. Do, C. Y. Tang, M. Reinhard, and J. O. Leckie, "Degradation of polyamide nanofiltration and reverse osmosis membranes by hypochlorite," *Environmental science & technology*, vol. 46, no. 2, pp. 852–859, 2012.

[12] M. J. Cran, S. W. Bigger, and S. R. Gray, "Degradation of polyamide reverse osmosis membranes in the presence of chloramine," *Desalination*, vol. 283, pp. 58–63, 2011.

[13] Y.-N. Kwon and J. O. Leckie, "Hypochlorite degradation of crosslinked polyamide membranes: I. changes in chemical/morphological properties," *Journal of membrane science*, vol. 283, no. 1, pp. 21–26, 2006.

[14] J. Glater, S.-k. Hong, and M. Elimelech, "The search for a chlorine-resistant reverse osmosis membrane," *Desalination*, vol. 95, no. 3, pp. 325–345, 1994.

[15] H. Shemer and R. Semiat, "Impact of halogen based disinfectants in seawater on polyamide ro membranes," *Desalination*, vol. 273, no. 1, pp. 179–183, 2011.

[16] T. Kawaguchi and H. Tamura, "Chlorine-resistant membrane for reverse osmosis. i. correlation between chemical structures and chlorine resistance of polyamides," *Journal of applied polymer science*, vol. 29, no. 11, pp. 3359–3367, 1984.

[17] J. Powell, J. Luh, and O. Coronell, "Bulk chlorine uptake by polyamide active layers of thin-film composite membranes upon exposure to free chlorine kinetics, mechanisms, and modeling," *Environmental science & technology*, vol. 48, no. 5, pp. 2741–2749, 2014.

[18] J. Glater, M. Zachariah, S. McCray, and J. McCutchan, "Reverse osmosis membrane sensitivity to ozone and halogen disinfectants," *Desalination*, vol. 48, no. 1, pp. 1–16, 1983.

[19] P. J. Vikesland, K. Ozekin, and R. L. Valentine, "Monochloramine decay in model and distribution system waters," *Water Research*, vol. 35, no. 7, pp. 1766–1776, 2001.

[20] Y. Bichsel and U. Von Gunten, "Oxidation of iodide and hypoiodous acid in the disinfection of natural waters," *Environmental science & technology*, vol. 33, no. 22, pp. 4040–4045, 1999.

[21] D. B. Jones, A. Saglam, H. Song, and T. Karanfil, "The impact of bromide/iodide concentration and ratio on iodinated trihalomethane formation and speciation," *Water research*, vol. 46, no. 1, pp. 11–20, 2012.

[22] "Amicon stirred cells: Ufsc05001." [Online]. Available: https://www.emdmillipore.com/US/en/product/Amicon-Stirred-Cells,MM_NF-C3259

[23] "Emd millipore ic millex nonsterile lh filter units, sllhc13nl." [Online]. Available: https://www.fishersci.com/shop/products/emd-millipore-ic-millex-nonsterile-lh-filter-units-2/sllhc13nl?searchHijack=true&searchTerm=SLLHC13NL&searchType=RAPID&matchedCatNo=SLLHC13NL

[24] "9mm non-assembled clear screw thread wide opening autosampler vial kits, 03-376-491." [Online]. Available: https://www.fishersci.com/shop/products/9mm-non-assembled-clear-screw-thread-wide-opening-autosampler-vial-kits/03376491?searchHijack=true&searchTerm=03376491&typeAheadCat=fisherCatNum&matchedCatNo=03376491

[25] "Copper conductive tape, double sided adhesive, 16074." [Online]. Available: http://www.tedpella.com/SEMmisc_html/SEMadhes.htm#anchor16074

[26] "Aluminum conductive tape." [Online]. Available: http://www.tedpella.com

[27] R. I. Urama and B. J. Mariñas, "Mechanistic interpretation of solute permeation through a fully aromatic polyamide reverse osmosis membrane," *Journal of membrane science*, vol. 123, no. 2, pp. 267–280, 1997.

[28] J. C. Crittenden, R. R. Trussell, D. W. Hand, K. J. Howe, and G. Tchobanoglous, *MWH's water treatment: principles and design*. John Wiley & Sons, 2012.

APPENDIX A

CHEMICAL PREPARATION

Table A.1: Sample calculations for monochloramine solution (1)

	Cl_2 Stock Solution	NH_4Cl Stock Solution
g NH_4Cl	—	1.001
concentration (M)	0.7060	0.749069276
concentration (mg/L)	50,055	20,020

Table A.2: Sample calculations for monochloramine solution (2)

Target MCA (ppm as Cl2)	Target MCA (M)	[NH4Cl] (M)	[HOCl] (M)	NH4Cl stock (M)	HOCl stock (M)
1000	0.01408	0.03098	0.02817	0.7491	0.7060
	Volume (mL)				
	50	25	25	1.034	0.997

Table A.3: Hypoiodous acid (HOI) and monochloramine (NH_2Cl concentrations

Desired CT		Time		Compound	Concentration Needed			
Value	Unit	Value	Unit		Value	Unit	Value	Unit
0.08	mM·h HOI	24	hour	I^-	3.33	μM	0.42	mg/L
				NH_2Cl	3.53	μM	0.25	mg/L
1	mM·h HOI	24	hour	I^-	0.04	mM	5.3	mg/L
				NH_2Cl	0.04	mM	3.0	mg/L
10	mM·h HOI	24	hour	I^-	0.42	mM	52.9	mg/L
				NH_2Cl	0.42	mM	30	mg/L
100	mM·h HOI	24	hour	I^-	4.17	mM	528.8	mg/L
				NH_2Cl	4.23	mM	300	mg/L
300	mM·h HOI	24	hour	I^-	12.5	mM	1586.3	mg/L
				NH_2Cl	12.7	mM	900	mg/L

Table A.4: UV-Vis Raw Data 1

Constants			
e	433.19	Path length (cm)	1

Experiment	UV Absorbance	Dilution	Concentration (M)	[MCA] stock (ppm)	Target [MCA] (ppm)	Volume Added (mL)	Reactor Volume (mL)
XPS	0.757	8	0.01398	992.5806	0.25	0.01259	50
XPS	0.7849	8	0.01449	1029.16	3	0.14575	50

Table A.5: UV-Vis Raw Data 2: 10 mM·h HOI Experiments

Constants			
e	433.19	Path length (cm)	1

Experiment	UV Absorbance	Dilution	Concentration (M)	[MCA] stock (ppm)	Target [MCA] (ppm)	Volume Added (mL)	Reactor Volume (mL)
Permeation	0.7849	8	0.014495256	1029.163185	30	1.45749481	50
	0.7602	8	0.014039105	996.7764722	30	1.504850929	50
RBS	0.7624	8	0.014079734	999.6611187	30	1.500508494	50
XPS	0.766	8	0.014146218	1004.381449	30	1.493456496	50
	0.7943	8	0.014668852	1041.488492	30	0.28804927	10

Table A.6: UV-Vis Raw Data 3: 100 mM·h HOI Experiments

Constants			
e	433.19	Path length (cm)	1

Experiment	UV Absorbance	Dilution	Concentration (M)	[MCA] stock (ppm)	Target [MCA] (ppm)	Volume Added (mL)	Reactor Volume (mL)
Permeation	0.757	8	0.013980009	992.5806228	300	15.11212254	50
	0.7943	8	0.014668852	1041.488492	300	2.880492701	10
RBS	0.7758	8	0.014327201	1017.231238	300	7.37295486	25
XPS	0.6159	8	0.011374224	807.5698885	300	18.57424381	50
	0.778	8	0.014367829	1020.115884	300	7.352105887	25

Table A.7: UV-Vis Raw Data 4: 300 mM·h HOI Experiments

Constants			
e	433.19	Path length (cm)	1

Experiment	UV Absorbance	Dilution	Concentration (M)	[MCA] stock (ppm)	Target [MCA] (ppm)	Volume Added (mL)	Reactor Volume (mL)
Permeation RBS XPS	0.7887	8	0.014565433	1034.145756	900	43.51417558	50
	0.778	8	0.014367829	1020.115884	900	44.11263532	50
	0.757	8	0.013980009	992.5806228	900	45.33636761	50
	0.7943	8	0.014668852	1041.488492	900	8.641478102	10
	0.7042	8	0.013004917	923.3491078	900	24.36781474	25
	0.7522	8	0.013891364	986.2868487	900	9.125134348	10

APPENDIX B

STRUCTURAL ANALYSES

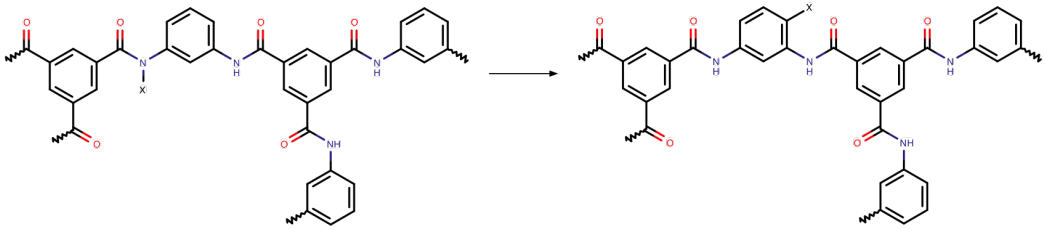

Figure B.1: Irreversible ring halogenation by Orton rearrangement. Initial chlorination of the amide nitrogen followed by rapid rearrangement to the aromatic ring. X represents the halogen (Cl, Br, I)

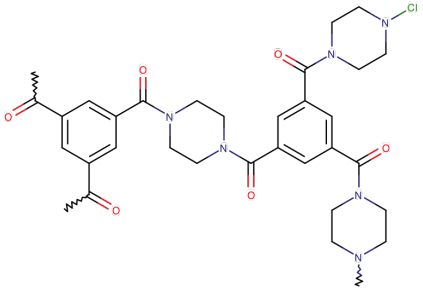

Figure B.2: Reversible chlorination of semi-aromatic polyamide membrane at the non-crosslinked nitrogen

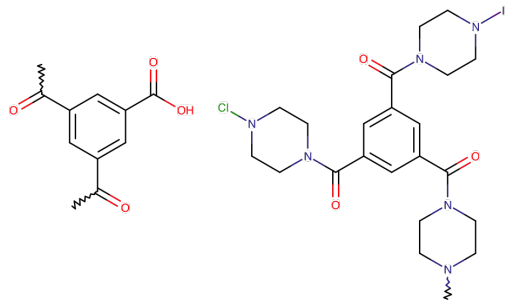

Figure B.3: C-N hydrolysis through chlorination of semi-aromatic polyamide membrane

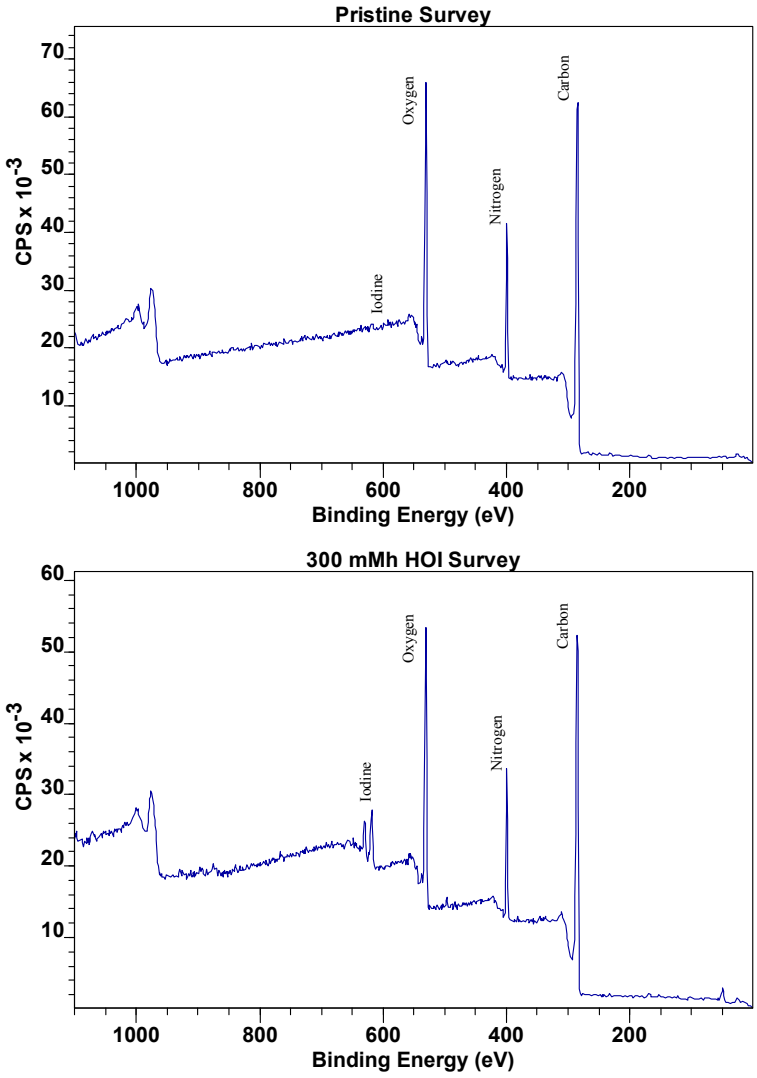

Figure B.4: XPS survey scans of pristine membranes (top) and 300 mM·h HOI exposed membranes (bottom)

Table B.1: Molar concentrations of iodine incorporated into membranes for permeation and non permeation experiments from RBS analysis

CT (mM·h HOI)	No Permeation		Permeation	
	NaI Rinse	NaCl Rinse	NaCl	R-WT
	I^- [M]			
10	0.0728	0.0520	0.0361	0.0208
100	—	0.1144	0.0586	0.0676
300	0.3328	0.2374	0.0639	0.1144

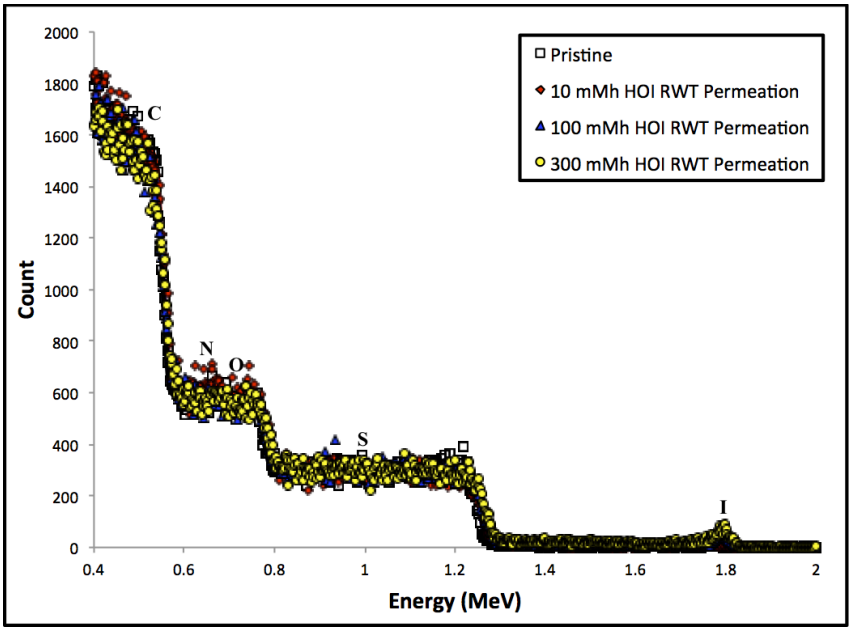

Figure B.5: RBS analysis of pristine, 10 mM·h HOI and 300 mM·h HOI exposed membranes followed by R-WT permeation - full spectra

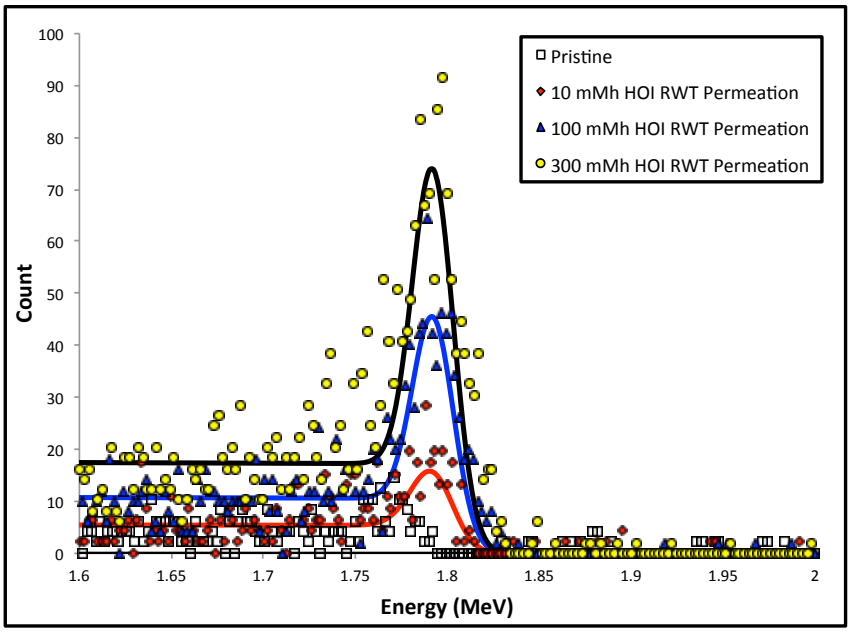

Figure B.6: RBS analysis of pristine, 10 mM·h HOI and 300 mM·h HOI exposed membranes followed by R-WT permeation - iodine spectra

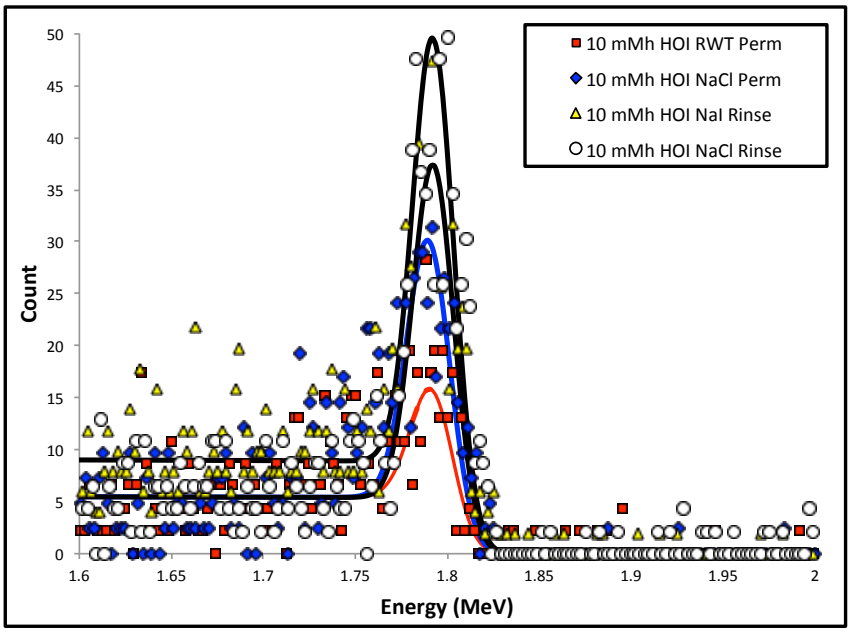

Figure B.7: RBS analysis of 10 mM·h HOI exposed membranes after NaI rinse, NaCl rinse, R-WT permeation and NaCl permeation

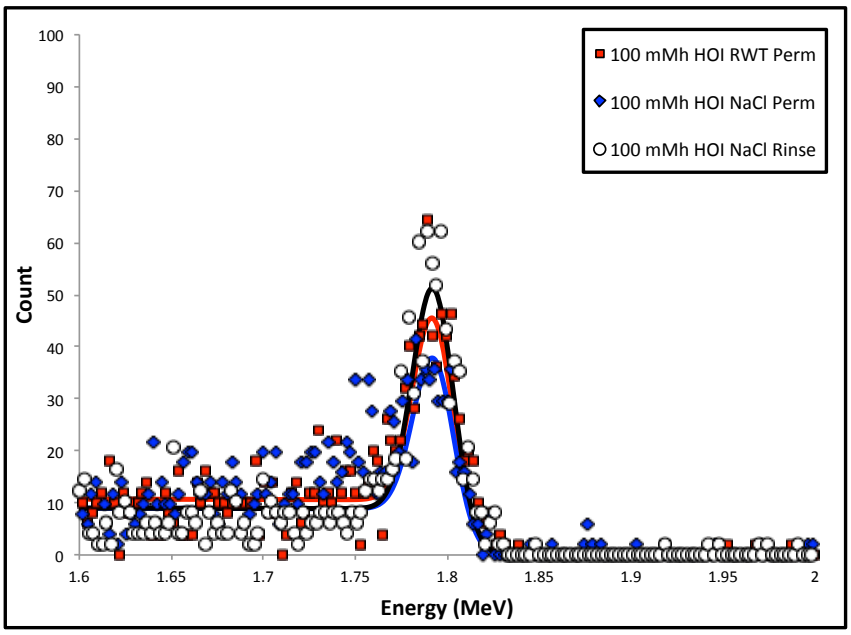

Figure B.8: RBS analysis of 100 mM·h HOI exposed membranes after NaCl rinse, R-WT permeation and NaCl permeation

APPENDIX C

PERFORMANCE ANALYSES

Table C.1: 10 mM·h HOI Pristine R-WT Rejection Raw Data

Pressure (MPa)	**Feed (mg/L)**	**Perm. 1 (mg/L)**	**Perm. 2 (mg/L)**	**Rej. (%) Perm. 1**	**Rej. (%) Perm. 2**	**Flux (m/d)**
0.07	2.83274581	0.10560394	0.108466736	96.27202909	96.17096827	0.24001394
0.0715	2.195109729	0.080084845	0.080742872	96.35167006	96.32169313	0.246427709
0.103	2.660342146	0.108395887	0.099174356	95.92549073	96.27212024	0.337008836
0.208	2.042370831	0.102209435	0.094879558	94.99554961	95.35444023	0.670179533
0.307	1.709694142	0.082736997	0.079435459	95.16071356	95.3538205	0.981913968
0.409	2.153844825	0.093482806	0.096714014	95.65972417	95.50970371	1.297228155

Table C.2: 10 mM·h HOI Exposed R-WT Rejection Raw Data

Pressure (MPa)	**Feed (mg/L)**	**Perm. 1 (mg/L)**	**Perm. 2 (mg/L)**	**Rej. (%) Perm. 1**	**Rej. (%) Perm. 2**	**Flux (m/d)**
0.077	2.700316561	0.093561572	0.092029138	96.53516283	96.59191299	0.27734547
0.109	2.763611242	0.112357242	0.107628767	95.93440494	96.10550263	0.38723836
0.208	2.173916085	0.109871802	0.107815905	94.94590418	95.04047531	0.71396443
0.307	2.476590237	0.125501513	0.122336954	94.93248778	95.06026665	1.0197015
0.403	1.795984399	0.089493678	0.089493678	95.01701251	95.01701251	1.33846658

Table C.3: 100 mM·h HOI Pristine R-WT Rejection Raw Data

Pressure (MPa)	**Feed (mg/L)**	**Perm. 1 (mg/L)**	**Perm. 2 (mg/L)**	**Rej. (%) Perm. 1**	**Rej. (%) Perm. 2**	**Flux (m/d)**
0.032	1.952291305	0.168220626	0.16737049	91.38342596	91.42697152	0.105031405
0.054	1.68917513	0.12356651	0.124067377	92.68480174	92.65515016	0.171469348
0.077	1.724135084	0.125600859	0.126451821	92.71513816	92.66578229	0.250003869
0.104	1.763818017	0.109307406	0.10078342	93.80279567	94.28606471	0.3429324
0.208	1.748641731	0.109307406	0.107343737	93.74901076	93.8613076	0.656173682
0.301	1.695912807	0.088003798	0.087959871	94.81083002	94.81342019	0.986010467
0.405	1.867162084	0.113077368	0.112102551	93.94389118	93.99609962	1.293390202

Table C.4: 100 mM·h HOI Exposed R-WT Rejection Raw Data

Pressure (MPa)	**Feed (mg/L)**	**Perm. 1 (mg/L)**	**Perm. 2 (mg/L)**	**Rej. (%) Perm. 1**	**Rej. (%) Perm. 2**	**Flux (m/d)**
0.032	1.972640701	0.116432038	0.116146353	94.09765608	94.11213847	0.091314704
0.055	2.104600191	0.142280781	0.138698208	93.23953396	93.4097598	0.169095699
0.07	1.983641524	0.110063318	0.107116441	94.45145121	94.60001016	0.226265375
0.11	1.990611511	0.095953209	0.083019264	95.17971195	95.82945926	0.348273235
0.205	2.034094154	0.095953209	0.101575721	95.28275481	95.00634124	0.625812121
0.301	1.788582657	0.100923901	0.102228716	94.3573253	94.28437283	0.944671997
0.401	1.777128365	0.076781378	0.071514419	95.67946925	95.97584395	1.325373145

Table C.5: 300 mM·h HOI Pristine R-WT Rejection Raw Data

Pressure (MPa)	**Feed (mg/L)**	**Perm. 1 (mg/L)**	**Perm. 2 (mg/L)**	**Rej. (%) Perm. 1**	**Rej. (%) Perm. 2**	**Flux (m/d)**
0.032	1.886415555	0.074033253	0.075613095	96.07545366	95.99170529	0.093788543
0.053	1.827725391	0.07537246	0.072199378	95.87616058	96.04976882	0.1674338
0.075	2.046855945	0.099084351	0.096140911	95.15919275	95.30299572	0.243719205
0.102	1.763418698	0.06606362	0.065599698	96.25366229	96.27997039	0.327212918
0.206	1.829941087	0.10130726	0.102220161	94.46390591	94.41401902	0.637515132
0.302	2.019391628	0.094177874	0.094118617	95.33632443	95.33925883	0.940846794
0.408	2.015819034	0.111003246	0.10192233	94.4933923	94.94387499	1.260244243

Table C.6: 300 mM·h HOI Exposed R-WT Rejection Raw Data

Pressure (MPa)	**Feed (mg/L)**	**Perm. 1 (mg/L)**	**Perm. 2 (mg/L)**	**Rej. (%) Perm. 1**	**Rej. (%) Perm. 2**	**Flux (m/d)**
0.03	1.882899843	0.091349517	0.092850797	95.14846648	95.06873416	0.089819412
0.053	1.819816696	0.104452977	0.102809677	94.26024737	94.35054765	0.174269757
0.07	1.855437206	0.074951697	0.072994963	95.96042935	96.06588878	0.213821715
0.109	1.79991743	0.074286847	0.070212699	95.87276364	96.09911555	0.341791048
0.202	1.928544299	0.106683181	0.107827595	94.46820171	94.40886088	0.614646399
0.301	1.910395508	0.112805218	0.108253654	94.09519035	94.33344283	0.913432843
0.409	1.783007184	0.119134506	0.11002923	93.31833843	93.82900806	1.218933912

Table C.7: 10 mM·h HOI Pristine NaCl Rejection Raw Data

Pressure (MPa)	**Feed (mg/L)**	**Perm. 1 (mg/L)**	**Perm. 2 (mg/L)**	**Rej. (%) Perm. 1**	**Rej. (%) Perm. 2**	**Flux (m/d)**
0.081	377.21995	236.59615	232.97105	37.27899333	38.23999765	0.208517597
0.106	721.48175	204.94125	202.7052	71.59439584	71.90432052	0.274029853
0.203	413.2685	142.39205	141.1268	65.54490604	65.85106293	0.551130068
0.305	436.8528	118.2784	119.21865	72.92488454	72.70965186	0.834115145
0.407	551.2329	105.08665	106.18835	80.93607076	80.73620969	1.182089561

Table C.8: 10 mM·h HOI Exposed NaCl Rejection Raw Data

Pressure (MPa)	**Feed (mg/L)**	**Perm. 1 (mg/L)**	**Perm. 2 (mg/L)**	**Rej. (%) Perm. 1**	**Rej. (%) Perm. 2**	**Flux (m/d)**
0.069	359.9722	251.7543	248.4131	30.0628493	30.99103209	0.179651363
0.108	310.32615	212.34185	211.94215	31.57461915	31.70341913	0.302650018
0.205	438.52895	157.0772	157.8079	64.18088247	64.01425721	0.5824915
0.301	547.11485	126.9975	128.1872	76.78778048	76.57033071	0.895522395
0.396	409.13425	107.27695	109.9989	73.77952347	73.1142284	1.176691047

Table C.9: 100 mM·h HOI Pristine NaCl Rejection Raw Data

Pressure (MPa)	**Feed (mg/L)**	**Perm. 1 (mg/L)**	**Perm. 2 (mg/L)**	**Rej. (%) Perm. 1**	**Rej. (%) Perm. 2**	**Flux (m/d)**
0.036	302.3106	269.53365	268.5529	10.84214381	11.16656181	0.118686568
0.055	332.30675	260.87745	259.89195	21.49498919	21.79155253	0.174253733
0.07	332.3882	235.7082	234.36165	29.08647178	29.49158544	0.222179106
0.104	363.91175	217.49355	217.3593	40.23453488	40.2714257	0.335113907
0.206	381.1615	176.92815	175.21055	53.58184129	54.03246393	0.657313438
0.307	407.0922	166.8745	167.3078	59.00818046	58.90174265	1.035223889
0.35	435.26235	174.09525	168.3607	60.00222624	61.31971902	1.164818773
0.403	408.69355	151.7946	153.02155	62.85857704	62.55836433	1.375522399
0.502	416.2094	139.18065	141.2983	66.55994555	66.05115118	1.730197032

Table C.10: 100 mM·h HOI Exposed NaCl Rejection Raw Data

Pressure (MPa)	**Feed (mg/L)**	**Perm. 1 (mg/L)**	**Perm. 2 (mg/L)**	**Rej. (%) Perm. 1**	**Rej. (%) Perm. 2**	**Flux (m/d)**
0.028	307.02145	264.3712	263.52885	13.89161897	14.16598091	0.085731344
0.049	329.63745	254.1235	257.1367	22.90818291	21.99408775	0.142878483
0.075	340.1428	250.97885	246.46915	26.21368143	27.53950694	0.223205631
0.106	348.9024	215.14985	216.5715	38.33523358	37.92777006	0.311641794
0.197	373.8904	172.36	173.7598	53.90092926	53.52654147	0.600526783
0.302	398.9614	181.96705	185.0834	54.38981064	53.60869498	0.955223888
0.345	420.00685	151.6779	154.9031	63.88680327	63.11891104	1.059275061
0.401	395.62575	136.12335	136.55245	65.59289935	65.48443826	1.246567174
0.498	414.0914	129.304	129.5315	68.7740436	68.71910404	1.552835833

Table C.11: 300 mM·h HOI Pristine NaCl Rejection Raw Data

Pressure (MPa)	**Feed (mg/L)**	**Perm. 1 (mg/L)**	**Perm. 2 (mg/L)**	**Rej. (%) Perm. 1**	**Rej. (%) Perm. 2**	**Flux (m/d)**
0.031	344.80075	279.77995	279.6897	18.85749958	18.88367412	0.086796786
0.052	348.3864	283.9427	284.35165	18.4977657	18.38038167	0.151952567
0.07	406.3749	254.2982	252.88555	37.42275913	37.77038149	0.197789824
0.104	352.3939	220.36215	218.67085	37.46709293	37.94703881	0.302553548
0.206	400.22115	172.35775	173.31165	56.93437241	56.69602918	0.607462691
0.303	402.30645	137.90495	139.5539	65.72141709	65.31154298	0.928358216
0.351	423.51095	127.858	128.90745	69.80998956	69.56219196	1.052003151
0.403	423.243	118.3756	119.6316	72.03129172	71.73453548	1.214328368
0.5	493.8502	103.97465	108.729	78.94611564	77.98340468	1.522388072

Table C.12: 300 mM·h HOI Exposed NaCl Rejection Raw Data

Pressure (MPa)	**Feed (mg/L)**	**Perm. 1 (mg/L)**	**Perm. 2 (mg/L)**	**Rej. (%) Perm. 1**	**Rej. (%) Perm. 2**	**Flux (m/d)**
0.035	298.24985	273.0393	271.4128	8.452829063	8.998177199	0.114357549
0.057	309.80505	249.74325	247.6988	19.38696609	20.0468811	0.175456054
0.08	328.01295	232.6093	233.8454	29.08533032	28.70848544	0.243402987
0.106	348.8965	218.6384	218.3596	37.33430975	37.41421883	0.316579268
0.2	382.468	180.07625	180.4136	52.91730289	52.82909943	0.601492542
0.3	427.468	153.6926	135.19115	64.04582331	68.37397185	0.946268664
0.357	456.3373	133.8528	129.8461	70.66801245	71.54602528	1.098614081
0.4	413.00925	128.627	124.2069	68.85614547	69.92636363	1.262686577
0.502	413.2156	120.4495	124.2069	70.85068908	69.94138169	1.601194043